Numerical Characterization of Three-Dimensional Serpentine Micromixers

Jang Min Park and Tai Hun Kwon
Dept. of Mechanical Engineering, Pohang University of Science and Technology (POSTECH), Nam-Gu, Pohang, Gyeongbuk 790-784, South Korea

DOI 10.1002/aic.11537
Published online June 11, 2008 in Wiley InterScience (www.interscience.wiley.com).

Three-dimensional serpentine micromixer (TSM) has been well known to be an attractive design because of its simple fabrication and efficient mixing performance, but its basic characteristics have not been fully investigated notwithstanding several reports in the past. The present article comprehensively investigates flow and mixing characteristics of TSM. Three major mixing mechanisms are identified, namely rotation, lamination, and chaotic advection. The mixing performance of TSM is analyzed and compared in terms of the three mechanisms by means of numerical analysis with three representative types as examples of TSM: (1) serpentine type C; (2) serpentine type L; (3) improved serpentine laminating micromixer. Numerical analysis system based on a finite element method and a colored particle tracking method enables not only flow visualization but also computation of Poincaré section and Lyapunov exponent for a dynamical system analysis of TSM. © 2008 American Institute of Chemical Engineers *AIChE J,* 54: 1999–2008, 2008
Keywords: microfluidics, mixing

Introduction

Microfluidic devices for miniaturized analytical systems such as a micro-total-analysis-system and lab-on-a-chip require a rapid mixing of fluids inside a microchannel.[1] One principal strategy for the rapid mixing is to increase the interfacial area of the fluids significantly by using stretching-reorientation, chaotic advection, and lamination via periodic perturbation, electrokinetics, split-and-recombine (SAR) flow, and so forth, since one cannot expect a turbulence mixing due to a low Reynolds number ($Re = UD/v$ where U, D, and v are characteristic values of the flow velocity, channel diameter, and kinematic viscosity, respectively) of the flow.[2] Various micromixers have been reported in the past two decades, and one can find comprehensive reviews in the literature.[2,3]

Generally, a micromixer with a simple geometry, easy operation, and efficient mixing performance is required for practical developments of the microfluidic chips, such as a disposable biochip.[4,5] Passive micromixers, in this regard, are more advantageous than active micromixers since their fabrication and operation are rather simple, thus its integration with other components along with the fabrication processes of the whole device can be more straightforward. Passive mixing strategies include the methods of using injection, chaotic advection, lamination (or SAR), recirculation, and so forth.[2,3] Many of such mixing mechanisms have been investigated experimentally or numerically. For example, Stroock et al.[1] developed a staggered herringbone micromixer (SHM) and demonstrated its chaotic mixing performance experimentally. More details of the flow and mixing characteristics of SHM were further investigated numerically by other researchers.[6–8] Schönfeld et al.[9] proposed an optimal design for SAR mixing via a computational fluid dynamics analysis, and their flow visualization result confirmed ideal lamellae structures of SAR micromixer in low Re regime. Helical flows due to a curvature effect inside a planar curved microchannel were also investigated for the chaotic mixing, both numerically and experimentally.[10,11] Two-dimensional ser-

Correspondence concerning this article should be addressed to T. H. Kwon at thkwon@postech.ac.kr.

pentine microchannels such as a planar zigzag microchannel were also reported to enhance the mixing with the help of the recirculation flow at the corner region for high *Re* regime, and the flow and mixing characteristics with different geometrical parameters were investigated.[12]

A three-dimensional serpentine micromixer (denoted as TSM), which is the main subject to be investigated in the present article, was first proposed by Liu et al.[4] to realize a rapid mixing, particularly with the help of the chaotic advection in the regime of $1 < Re < 100$. A "C"-shaped mixing unit (STC), shown in Figure 1a, was utilized in this micromixer, and their experimental mixing results showed a significant advection effect enhancing the mixing performance as *Re* increases. Also, mixing performances of a two-dimensional square-wave micromixer and STC were compared with various *Re* in their experiments, and the results confirmed a much higher mixing performance of TSM. Another TSM using an "L"-shaped mixing unit (STL), shown in Figure 1b, was utilized by Vijayendran et al.[13] for a biosensor application. Fluid elements rotate as passing through STL channel, which results in a series of twist of fluid elements. Both STC and STL are advantageous in terms of an efficient mixing performance by the significant advection effect with a simple design, thus they have been employed by several researchers in developing novel micromixers. For example, Kim et al.[14] utilized the serpentine geometry in their serpentine laminating micromixer (SLM), which consists of "F"-shaped mixing units. SLM was aimed to combine two mixing mechanisms of advection and lamination with a simple design enabling mass production via injection molding. SLM was further improved by narrowing the merging zone of F-shape element, named improved SLM (ISLM).[14,15] Since lamination mechanism was introduced additionally in their development, a high level of mixing can be achieved for a wide range of *Re*. Xia et al.[16] also introduced the serpentine geometry in a two-layer crossing channel (denoted as TLCCM in their article), which exhibits a fast mixing by the chaotic advection even in low *Re* regime. The inertia effect on the mixing performance of TLCCM was further investigated in more detail using a dynamical analysis technique.[17] Chen and Meiners[18] proposed a Möbius band-like micromixer, which is designed to achieve a fast mixing by the lamination within a low *Re* regime, and in this micromixer also, the serpentine geometry was utilized.

Although TSM has an important potential for the micromixer developments as mentioned earlier, a detailed analysis of its basic flow and mixing characteristics has not been fully established. In this regard, the present article comprehensively investigates flow and mixing characteristics of TSM. Through this study, three major mixing mechanisms are identified: namely rotation, lamination, and chaotic advection. The mixing performance of TSM is analyzed in terms of the three mechanisms by means of numerical analysis. For this purpose, three representative types are chosen as examples of TSM: (1) STC; (2) STL; and (3) ISLM. Numerical analysis system is developed based on a finite element method and colored particle tracking method (CPTM) to obtain velocity field and flow visualization. Poincaré section and Lyapunov exponent are also employed for a dynamical system analysis.[7,17,19]

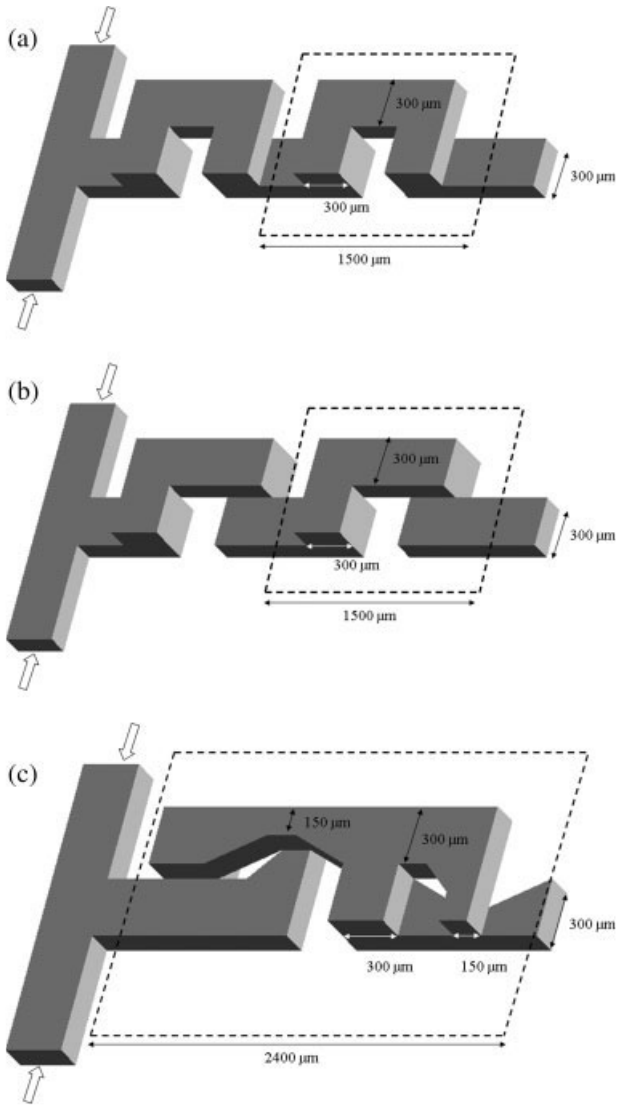

Figure 1. Schematics of (a) STC, (b) STL, and (c) ISLM.

Three-Dimensional Serpentine Micromixers

Three representative types of TSM are introduced briefly with corresponding schematics in this section. Figure 1a shows STC which consists of "C"-shaped units arranged in a spatially periodic manner along the downchannel direction. Similarly, Figure 1b shows an STL that has L-shaped units and Figure 1c shows ISLM with F-shaped units. STC and STL are fundamental designs of TSM using only the simplest three-dimensional serpentine geometry in two layers. ISLM, on the other hand, introduces additional stream paths for SAR mechanism (ISLM in Figure 1c is a slightly modified version of the previous ISLM with a more compact channel design while keeping its mixing mechanisms unchanged).[15] Since the performances of TSM have been investigated mostly via microfluidic mixing visualization experiments, of which characterization methods are based on evaluation of a mixing intensity or standard deviation, the basic characteristics of TSM could not be fully analyzed in detail in the past

researches. Because of the lack of theoretical or numerical analysis of TSM, three-dimensional flow fields and mixing mechanisms have not been completely clarified yet.

In this regard, comprehensive investigations on TSM are carried out with the three examples (STC, STL, and ISLM) via numerical methods. Particularly, two different channel aspect ratios of 0.2 and unity are considered for each design of the micromixers, and the channel aspect ratio will be noted as one of the most important geometric parameters of TSM. Detailed length scales of the micromixers are indicated in Figure 1 (channel depths are 60 and 300 μm for the channel aspect ratios of 0.2 and unity, respectively).

Numerical Analysis Method

Numerical analysis system is developed based on a finite element method and CPTM to investigate the flow and mixing characteristics of TSM. Finite element analysis provides solutions of flow fields inside the micromixers in detail. CPTM enables visualization of the flow and consequent mixing behaviors in terms of particle trajectories and cross-sectional particle distributions along the downchannel.[7] CPTM is also utilized to obtain Poincaré sections and Lyapunov exponents of the micromixers.[7,17,19]

Numerical analysis is carried out on periodic mixing units (inside dashed boxes in Figure 1) instead of the whole domain of micromixers, since the velocity field can be assumed to have a period per mixing unit because of their spatially periodic design along the downchannel direction. Once the velocity field inside the mixing unit is given, one can obtain particle trajectories via time integrations of the velocity field. Governing equations for a steady state incompressible flow is represented by Eq. 1, which is solved numerically by the finite element method. Here, ρ, $\mathbf{u}$, p, μ, and $\boldsymbol{D}$ denote the density, velocity vector, hydrostatic pressure, dynamic viscosity, and the rate of deformation tensor, respectively.

$$\begin{cases} \rho(\mathbf{u}\cdot\nabla)\mathbf{u}+\nabla p-\nabla\cdot(2\mu\boldsymbol{D})=\mathbf{0} \\ \nabla\cdot\mathbf{u}=0 \end{cases} \tag{1}$$

No-slip boundary condition at the channel wall (Γ_w), and traction boundary condition at the inlet and the outlet (Γ_i and Γ_o, respectively) are represented by Eq. 2. Δp is a pressure drop between the inlet and outlet, $\mathbf{t}$ and $\mathbf{n}$ are traction vector and outward normal vector on a surface, respectively.

$$\begin{cases} \mathbf{u}=0 & \text{on } \Gamma_w \\ \mathbf{t}=-\Delta p\mathbf{n}+2\mu\boldsymbol{D}\cdot\mathbf{n} & \text{on } \Gamma_i \\ \mathbf{t}=2\mu\boldsymbol{D}\cdot\mathbf{n} & \text{on } \Gamma_o \end{cases} \tag{2}$$

In order to take the periodic condition of the mixing units into account, velocities at the inlet and outlet are constrained to be identical as represented by Eq. 3.

$$\mathbf{u}_{in}=\mathbf{u}_{out} \tag{3}$$

The stabilized finite element formulation for the governing equations, boundary conditions, and a constraint (Eqs. 1–3) can be stated as Eq. 4, where $\mathbf{v}$ and q are weighting functions for the velocity and pressure, respectively, τ and δ are stabilization parameters.[20,21] λ is a Lagrange multiplier function and φ is a corresponding weighting function.[7]

$$\begin{aligned} &\int_\Omega 2\mu\boldsymbol{D}(\mathbf{u})\cdot\boldsymbol{D}(\mathbf{v})\,d\Omega+\int_\Omega\rho(\mathbf{u}\cdot\nabla\mathbf{u})\cdot\mathbf{v}\,d\Omega-\int_\Omega p(\nabla\cdot\mathbf{v})\,d\Omega \\ &+\int_\Omega q(\nabla\cdot\mathbf{u})\,d\Omega+\sum_K\int_{\Omega_K}(\nabla\cdot\mathbf{u})\delta(\nabla\cdot\mathbf{v})\,d\Omega_K \\ &+\sum_K\int_{\Omega_K}\left(\rho\mathbf{u}\cdot\nabla\mathbf{u}+\nabla p-\nabla\cdot\left[2\mu\boldsymbol{D}(\mathbf{u})\right]\right)\cdot \\ &\tau\left(\rho\mathbf{u}\cdot\nabla\mathbf{v}+\nabla q-\nabla\cdot\left[2\mu\boldsymbol{D}(\mathbf{v})\right]\right)d\Omega_K \\ &+\sum\left[\varphi(\mathbf{u}_{in}-\mathbf{u}_{out})+\lambda(\mathbf{v}_{in}-\mathbf{v}_{out})\right]=\int_{\Gamma_i\cup\Gamma_o}\mathbf{t}\cdot\mathbf{v}\,d\Gamma \end{aligned} \tag{4}$$

Table 1. Total Numbers of Elements and Nodes for Each Mixing Unit

Mixing Unit (Channel Aspect Ratio)	No. of Elements	No. of Nodes
STC (unity)	243,000	260,431
STC (0.2)	48,600	57,319
STL (unity)	243,000	260,431
STL (0.2)	48,600	57,319
ISLM (unity)	478,800	511,283
ISLM (0.2)	102,600	120,497

Computational domains are discretized by cubic elements for which trilinear interpolations are employed for both velocity and pressure fields. Total numbers of elements and nodes used for the domain discretization can be found in Table 1 for each mixing unit, for two channel aspect ratios of 0.2 and unity.

Two species of red and blue particles are introduced at the inlet of the mixing unit, and one can visualize the flow and mixing behaviors by tracking their trajectories. The particle trajectories are obtained by fourth order Runge-Kutta explicit time integration of the particle velocity field. Also, the particle tracking method is utilized to achieve the Poincaré section and Lyapunov exponent. Poincaré section can be obtained by recording every intersection of the particle trajectories with the outlet surface for an infinitely long period of the mixing unit, and finally plotting all the intersections in a single map.[22] The more the number of periods, the better the Poincaré section becomes. In the real computation of the Poincaré section, the present study used 100 periods which is believed to be sufficient. Poincaré section enables us to visualize the three-dimensional flow characteristics and mixing performances in a two-dimensional plot. Quantitative characterization of the mixing performance is carried out by evaluating Lyapunov exponents. The Lyapunov exponent represents a degree of divergence of initial conditions in the system as time goes on.[22] If the Lyapunov exponent is larger than zero, the initial conditions with a little difference will diverge exponentially with time, i.e. the system exhibits a chaotic behavior, while null Lyapunov exponent represents a stable system. Recently, Xia et al.[17] proposed a numerical method to evaluate the Lyapunov exponent which is simple

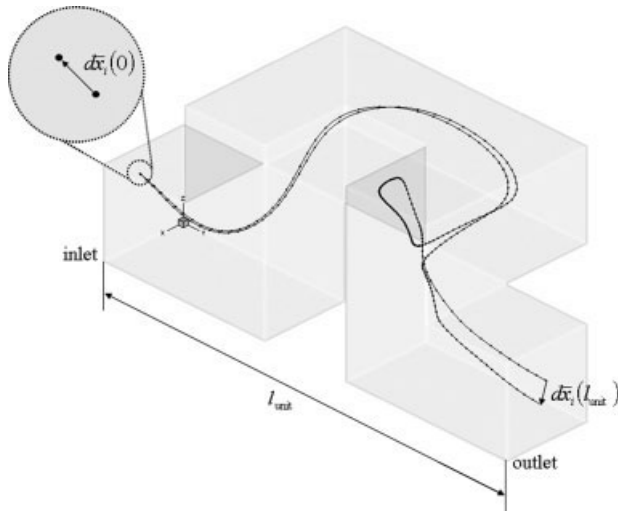

Figure 2. Trajectories of adjacent two particles along STC with a channel aspect ratio of unity when *Re* = 100.

and directly applicable to the three-dimensional periodic mixing units. In the present study, the Lyapunov exponent is evaluated by the similar manner as Xia et al.[17] proposed. Shown in Figure 2 are trajectories of two particles, denoted by the position vectors, $(x_{i,1}, 0, z_{i,1})$ and $(x_{i,2}, 0, z_{i,2})$ at the inlet surface. A small element vector is then represented by $\mathbf{dx_i}(0) = (x_{i,2} - x_{i,1}, 0, z_{i,2} - z_{i,1})$ at the inlet surface. If the flow exhibits a chaotic behavior, the paths of these adjacent particles would become significantly different from each other, such that the distance of the two particles $|\mathbf{dx_i}(y)|$ increases exponentially with the downchannel direction y. The Lyapunov exponent γ_i of an initial condition $\mathbf{dx_i}(0)$ is evaluated as a logarithmic ratio of distance between two particles at the inlet and outlet as

$$\gamma_i = \frac{1}{l_{\text{unit}}} \ln \frac{|\mathbf{dx_i}(l_{\text{unit}})|}{|\mathbf{dx_i}(0)|} \tag{5}$$

where i is an index for the initial location of a particle pair, l_{unit} is a total downchannel length of a mixing unit. It may be mentioned that Xia et al.[17] used unity for l_{unit} in the real calculation of γ_i for different kinds of micromixers, whereas in the present study, actual values of l_{unit} are used for fair comparison of mixing performances with a consideration of the different lengths of the mixing units (l_{unit} is 0.15 cm for STC and STL, and 0.24 cm for ISLM as shown in Figure 1). As a characteristic value of the mixing performance, average Lyapunov exponents (γ) are evaluated, which can be represented as

$$\gamma = \frac{1}{N} \sum_{i=1}^{N} \gamma_i \tag{6}$$

where N is the total number of initial vectors $\mathbf{dx_i}(0)$. The average Lyapunov exponent has a close correlation with a specific stretching per period introduced by Hobbs and Muzzio.[23,24] In this study, 18,000 and 90,000 vectors (i.e. 36,000 and 180,000 particles), respectively for channel aspect ratios of 0.2 and unity, are used with uniformly distributed locations in the inlet. The initial vector $\mathbf{dx_i}(0)$ is chosen as $\mathbf{dx_i}(0) = |\mathbf{dx_i}(0)|(2^{-1/2}, 0, 2^{-1/2})$, where the magnitude $|\mathbf{dx_i}(0)|$ has an order of 10^{-8} m. As mentioned earlier, such an infinitesimally small distance in the initial conditions can increase exponentially if the mixing unit induces a chaotic behavior.

Flow and Mixing Characteristics

Stokes flow regime characteristics

In this section, Stokes flow regime ($Re < 1$) characteristics of TSM are investigated, particularly with the help of cross-sectional particle distributions and interface trajectories in the following manner. Two different colors are introduced: red and blue ones to represent particles in the left half and right half of the inlet surface, respectively. Consequently, an interface is formed in the vertical direction (z-direction) in the inlet surface, when $-y$ direction is taken as a view direction. This interface will be deformed in the downchannel direction.

First, let us consider the cases with a channel aspect ratio of 0.2. Shown in Figure 3 are trajectories of the interfaces along the downchannel direction (Figure 3a), cross-sectional colored particle tracking results at two locations of $y = 0.5\ l_{\text{unit}}$ and $y = l_{\text{unit}}$ (Figure 3b), and conceptual diagrams describing the flow characteristics of each micromixer (Figure 3c). For the case of STC, the initially vertical interface in the inlet is rotated about y-axis in a negative direction (i.e. clockwise rotation) after the first serpentine region. As a result of this rotation, one can observe a tilted thus stretched interface at $y = 0.5\ l_{\text{unit}}$. θ indicated in Figure 3c denotes a magnitude of the rotation angle and it is about 30° for STC. Then the interface returns back to its initial configuration at $y = l_{\text{unit}}$ because of a positive rotation about y-axis (counterclockwise direction) by the second serpentine region. STL also exhibits the rotational motion about y-axis in the negative direction at the first serpentine region. However, in contrast to STC, the second serpentine region of STL rotates the fluid element again in the same (i.e. negative) direction, resulting in a further tilted and stretched interface at the outlet as indicated in Figure 3b for STL. As discussed earlier, one should note that STC and STL possess quite different flow characteristics in Stokes flow regime: STC periodically perturbs the flow field, such that clockwise and counterclockwise rotations occur alternatively with a canceling effect, resulting in no stretching of the interface; however, STL induces clockwise rotations successively so that the interface will be twisted continuously (thus stretched continuously as in the case of an upper-lid driven cavity flow)[22] along the downchannel. In this regard, STL would have rather higher mixing performance than STC in Stokes flow regime because of the continuous stretching of the interface by successive rotations. Now let us pay attention to ISLM. In ISLM, not only the rotation but also SAR mechanism contributes to the mixing in combination. SAR mechanism of ISLM is realized by introducing additional two stream paths, as depicted by dashed blue lines in Figure 3c. Without these additional stream paths, ISLM would be the same as STL, except that the rotations are in different directions. In this regard, F-shape unit of ISLM can be regarded as one variational design

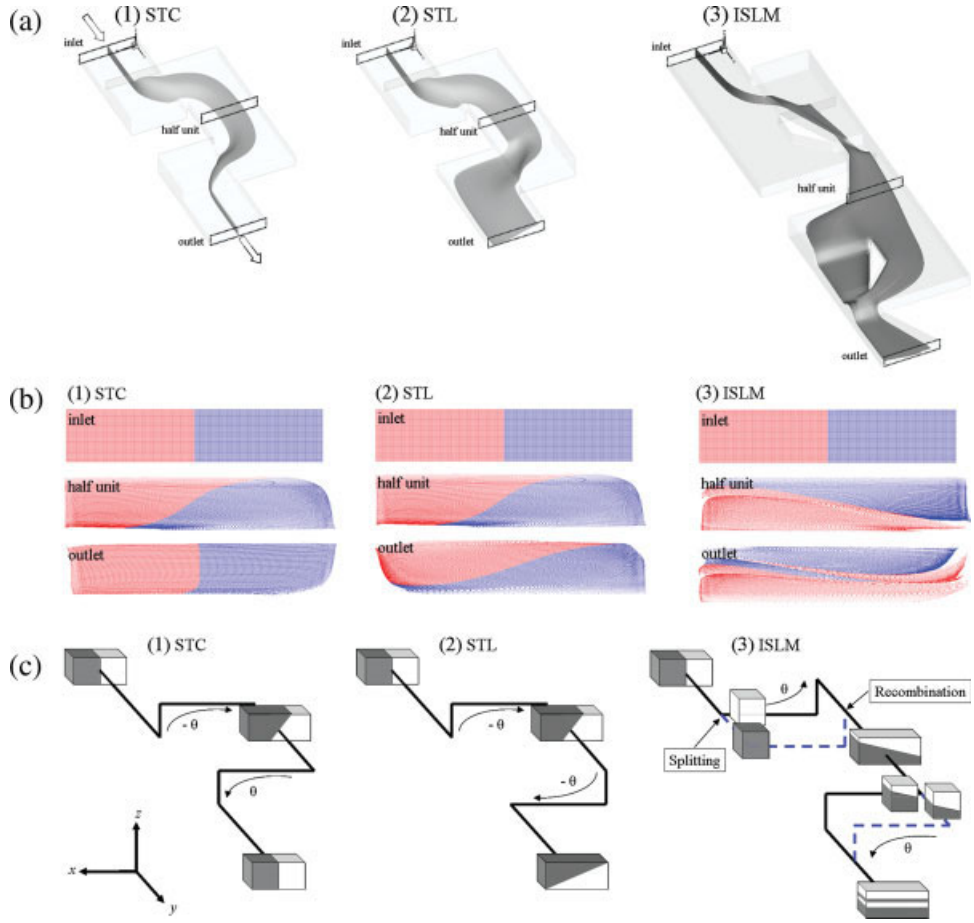

Figure 3. Comparisons between three representative types of TSM.

(a) Interface trajectories, (b) cross-sectional colored particle distributions, and (c) conceptual diagrams of the flow characteristics in a Stokes flow regime when channel aspect ratio is 0.2 for each design. [Color figure can be viewed in the online issue, which is available at www.interscience.wiley.com.]

of L-shape unit of STL. SAR mechanism in combination with the rotation results in a horizontally stretched interface after the first recombination region. Second SAR paths also work in the same manner, consequently resulting in a lamellae configuration at the end of one unit (Figure 3b). This process of achieving the lamellae configuration is termed a lamination, noted as one of the flow and mixing characteristics in the present study. As a result, ISLM increases the interfacial area most significantly among the three designs of TSM.

Now, let us consider a case with the channel aspect ratio of unity in Figure 4. In this figure, one can again observe rotations which have similar tendencies shown in Figure 3. However, a big difference lies in a degree of the rotation angle θ. In this case, θ turns out to be almost 90°, which is significantly larger than that of the channel aspect ratio of 0.2 in Figure 3b. However, the rotational directions remain the same. From these results, one can deduce two important features of rotation as follows: a bending sequence of the stream path (i.e. a channel orientation) at serpentine region determines the rotational direction; and the channel aspect ratio affects the rotational angle significantly in such a way that the lower the aspect ratio (lower than unity), the less the rotational angle. In other words, the difference in the rotational direction of STC and STL at the second serpentine region is because of difference in the bending sequence, and increase in the rotational degree of STC (or STL) from Figures 3 to 4 is due to the increase in the channel aspect ratio. The flow characteristics of STC and STL remain the same as the case of the lower aspect ratio, but with higher rotational angle. As far as ISLM is concerned, the larger rotational degree turns out to deteriorate the lamination performance as indicated in Figure 4 compared with Figure 3. One can observe only rotated configuration with a slight distortion of the interface after one unit (Figure 4b) in contrast to the lamellae configuration shown in Figure 3b. Though SAR mechanism does split and recombine the streams, the lamination cannot be achieved because of successive reorientations of cross-sectional configurations by the larger rotations. This combined procedures of SAR and rotation can be understood better with the help of three figures, Figures 4a-3, b-3, and c-3 for ISLM. The green line plotted in Figure 4c-3 represents the border line between materials coming from the left half and right half portions after the second split. During the second recombination, those two portions rotate 90° in a coun-

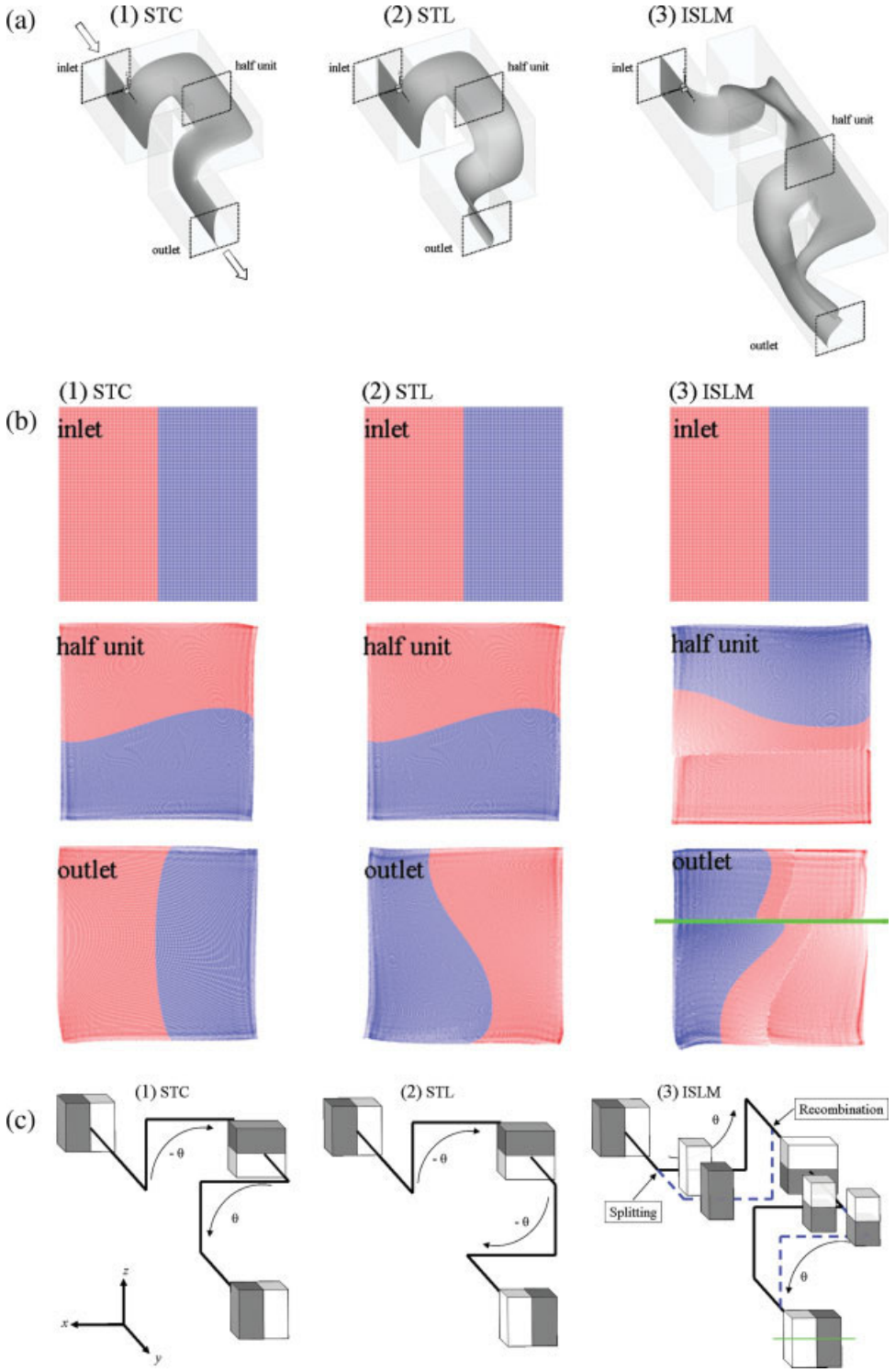

Figure 4. Comparisons between three representative types of TSM.

(a) Interface trajectories, (b) cross-sectional colored particle distributions, and (c) conceptual diagrams of the flow characteristics in a Stokes flow regime when channel aspect ratio is unity for each design. [Color figure can be viewed in the online issue, which is available at www.interscience.wiley.com.]

terclockwise direction, being combined at the end of one unit in such a way that the left and right half portions lie in the bottom and the top, respectively. According to the real simulation, the green line is also plotted in Figure 4b-3. In this case with the channel aspect ratio of unity, a micromixer proposed by Chen and Meiners[18] would be a better design to achieve a lamination instead of ISLM. In contrast, when the channel aspect ratio is reduced to say 0.2, the lamination per-

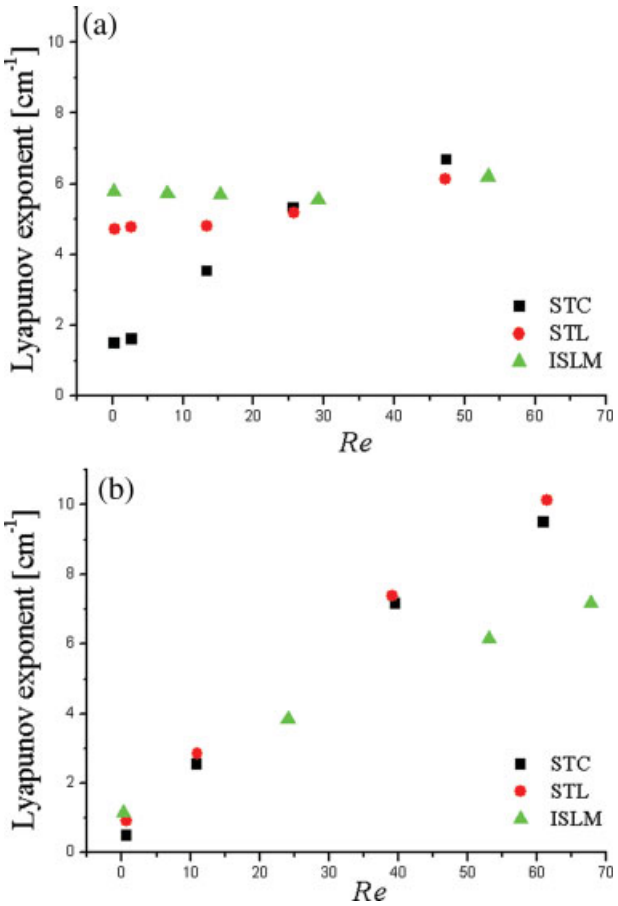

Figure 5. Plots of averaged Lyapunov exponents as *Re* changes for each design with a channel aspect ratio of (a) 0.2 and (b) unity.

[Color figure can be viewed in the online issue, which is available at www.interscience.wiley.com.]

formance of the micromixer by Chen and Meiners[18] will be deteriorated, while ISLM achieves the lamination as shown in Figure 3. The aspect ratio in most microfluidic chips is usually small (order of 0.1), since the depth is in order of 10 μm while the width is in order of 100 μm.[2] In this respect, ISLM seems more suitable for such microfluidic chips.

Lyapunov exponents and Poincaré sections

Shown in Figure 5 are the average Lyapunov exponents with changing *Re* for each design of TSM (Figures 5a, b are for channel aspect ratio of 0.2 and unity, respectively). And shown in Figures 6 and 7 are Poincaré sections of TSM with channel aspect ratios of 0.2 and unity, respectively, for several *Re* regimes.

Most microfluidic chips have a low aspect ratio (of order of 0.1) microchannel and operate in the Stokes flow regime (i.e. $Re \ll 1$). In this regard, one may be interested in investigating the mixing performance for such cases. According to Figure 5a for the case of aspect ratio of 0.2, the Lyapunov exponents are largest for ISLM and smallest for STC at low *Re* regime. The largest Lyapunov exponents for ISLM are due to the lamination mechanism, while the medium value for STL is attributed to the twisting effect due to continuous rotation. The poor performance of STC at low *Re* reflects that the present alternating rotations cannot stretch the material element significantly due to some canceling effects. As *Re* increases, however, the alternating rotations do not cancel any more due to inertia effects, and in this way chaotic advection is induced such that the increase of Lyapunov exponents is most obvious in the case of STC. STL also shows mixing enhancement as *Re* increases with the help of advection effects. Particularly in ISLM, lamination effect dominates the mixing mechanism with relatively insignificant contribution of advection. Thus, at high *Re* regime, the Lyapunov exponents become most similar to each other. These results qualitatively agree with previous experimental results in that STC and STL enhance the mixing as *Re* increases,[4,13] and that ISLM achieves high level of mixing over a wide range of *Re*.[14,15]

Presented in Figure 5b are Lyapunov exponents in the case of high aspect ratio of unity. The trends in Figure 5b are different from those for low aspect ratio when compared with Figure 5a. The difference in Lyapunov exponents at low *Re* is not as great as that for the low aspect ratio case, even if the order of values among STC, STL, and ISLM remains the same. In the high aspect ratio, the advection effect becomes the most dominating one as *Re* increases for all three designs. The main reason is that as channel aspect ratio increases from say 0.2 to unity, the vertical (z-directional) advections would be significantly strengthened, resulting in more effective stirring. Particularly, a large width-to-depth ratio (low channel aspect ratio) seems to be more effective

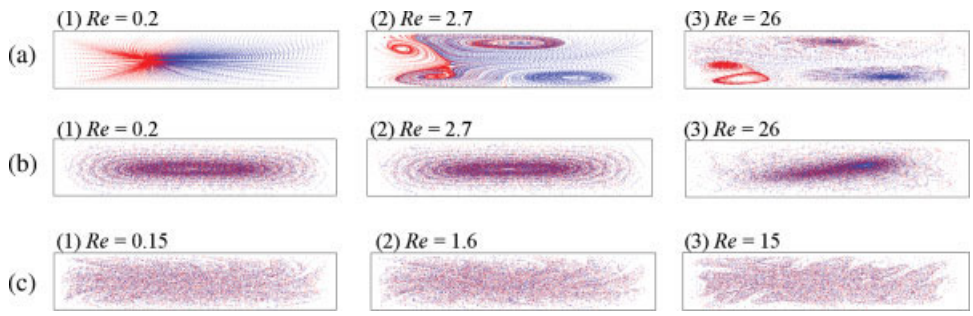

Figure 6. Poincaré sections of (a) STC, (b) STL, and (c) ISLM with a channel aspect ratio of 0.2 for various *Re*.

[Color figure can be viewed in the online issue, which is available at www.interscience.wiley.com.]

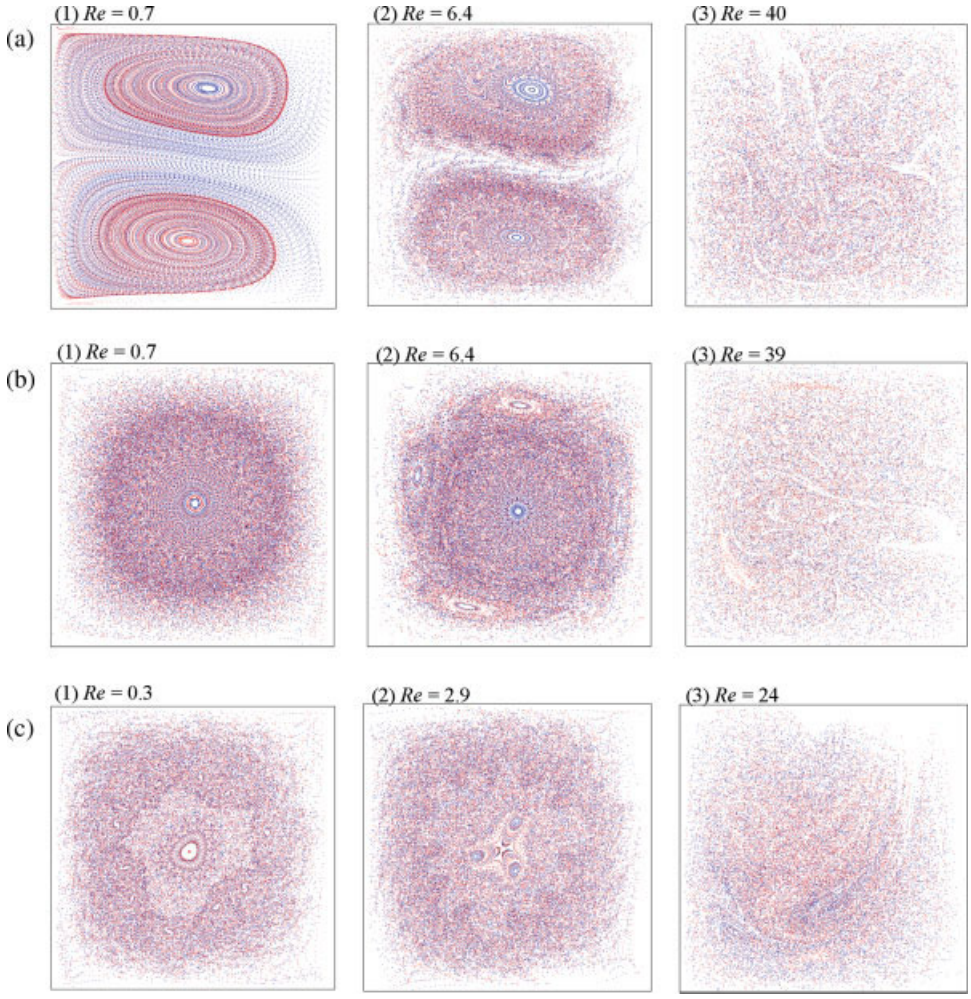

Figure 7. Poincaré sections of (a) STC, (b) STL, and (c) ISLM with a channel aspect ratio of unity for various *Re*.

[Color figure can be viewed in the online issue, which is available at www.interscience.wiley.com.]

for the stretching mechanism of STL since Lyapunov exponents for STL turns out to vary with the aspect ratio quite significantly at low *Re*. Now, as for ISLM, the lamination effect is weak in this case as expected from the results shown in Figure 4c-3. It may be pointed out that the mixing performance of ISLM with high aspect ratio looks poorest at high *Re* amongst the three designs, which is not, however, of critical concern since the range of operation and aspect ratio is not practical in the real microfluidic chips. In Table 2, the mixing mechanisms of three kinds of TSM are summarized.

As shown in Figures 6 and 7, Poincaré sections also visualize the enhanced chaotic behavior as *Re* increases. It is a well-known feature of TSM that as *Re* increases advections enhance the mixing performance by stirring the flow (thus stretching and folding the fluids), which is usually referred to as a chaotic advection in the literature.[2,4,13,14] First, let us pay attention to the case of the low aspect ratio, for which the Poincaré sections are plotted in Figure 6. Poincaré section results in Figure 6a clearly indicate the mixing characteristics of STC by showing a poor mixing (almost no mixing in fact) at $Re = 0.2$ and more uniform mixings as *Re* increases. As noted in the previous section, the alternating rotation in STC cannot enhance the mixing at low *Re* because of the canceling effect, and inertia effect plays a more significant role of inducing the chaotic advection as *Re* increases. As a matter of fact, as *Re* increases in Figure 6a, one can observe four large Kolmogorov-Arnold-Moser (KAM) tori at $Re = 3.3$ and four smaller KAM tori at $Re = 26$. It is well known that materials inside a KAM torus remain inside, thus preventing chaotic mixing from happening inside. These KAM tori may reflect the three-dimensional swirling flows due to the advections. The chaotic region gets larger with diminishing size of KAM tori as *Re* increases in Figure 6a. In the case of STL, Figure 6b shows visibly an elliptic point near the center, which indicates the continuous twisting effect. Figure 6c confirms the chaotic mixing of

Table 2. Mixing Mechanisms of Three Types of TSM

Mixing Unit	Mixing Mechanism
STC	Chaotic advection
STL	Rotation, chaotic advection
ISLM	Rotation, lamination, chaotic advection

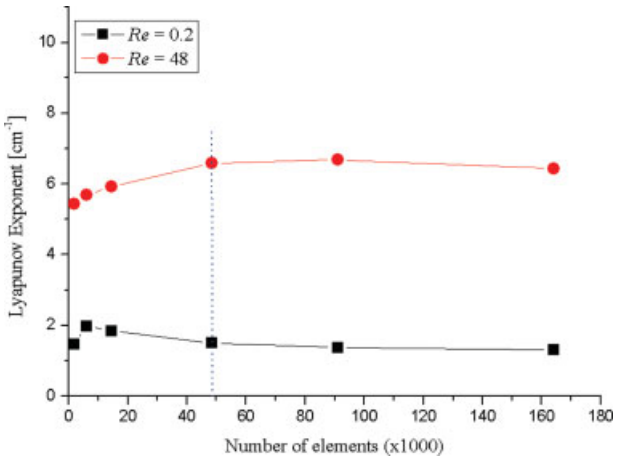

Figure 8. Mesh convergence test result with low aspect ratio STC for *Re* of 0.2 and 48.

[Color figure can be viewed in the online issue, which is available at www.interscience.wiley.com.]

ISLM in the whole range of *Re*. Now, let us discuss the high aspect ratio case, for which Poincaré sections are plotted in Figure 7. As opposed to the low aspect ratio case, STC has two visible elliptic points with two counterrotating flows at $Re = 0.7$ as shown in Figure 7a. As *Re* increases, regions for two elliptic point get smaller and many KAM tori appear with increasing chaotic region at $Re = 6.4$ and finally most region becomes chaotic at $Re = 40$. As for STL case, there is one elliptic point near the center at $Re = 0.7$, and one elliptic point near the center with four higher order elliptic points at $Re = 6.4$, indicating improved chaotic mixing compared with the case of $Re = 0.7$. At $Re = 39$ for STL, most region becomes chaotic. In the case of ISLM, at $Re = 0.3$, one can find 1 elliptic point near the center and 11 small KAM tori while there are 3 KAM tori with higher order chaotic structures at $Re = 2.9$. Again at $Re = 24$, most region becomes chaotic in ISLM, too.

Since finite element solution and particle tracking method can be influenced by the refinement of mesh, a mesh convergence test of the Lyapunov exponent is also carried out with a low aspect ratio STC for two *Re* of 0.2 and 48. Five additional mesh systems having different number of elements are employed for the test, and Figure 8 shows the result in terms of the Lyapunov exponent vs. number of elements. In this figure, dotted line indicates the present mesh condition. The convergence of Lyapunov exponent is clearly shown in this figure, and the present mesh condition is in the reliable region providing almost converged Lyapunov exponents with a moderate computational time.

Concluding Remarks

In this study, the flow and mixing characteristics of TSM are numerically investigated by using three representative micromixers of STC, STL, and ISLM. Particularly, three characteristics of rotation, lamination, and chaotic advection are identified and noted as main features of TSM. Also, as a result of the present investigation, different mixing mechanisms employed in STC, STL, and ISLM could be clarified further in detail. Followings summarize the characterization results.

- Three-dimensional serpentine stream path induces rotation of fluid about downstream axis in a positive or negative direction.
- The rotation direction depends on a bending sequence (channel orientation) of the serpentine region, and degree of the rotation depends on a channel aspect ratio.
- Lamination by SAR mechanism can be achieved by introducing additional stream paths in a proper manner, of which channel design should take the rotation effects into account.
- Chaotic advection can significantly enhance the mixing as *Re* increases, and the lower the channel aspect ratio (lower than unity) the less effective the advection.

With these characteristics, mixing mechanisms of three micromixers (STC, STL, and ISLM) are summarized as follows.

- STC can induce a chaotic advection with the help of inertia effect breaking the symmetry of the alternating rotational flows.
- STL has not only continuous twisting effect by successive rotational flow, but also chaotic advection by inertia effect.
- ISLM has three mixing mechanisms of rotation, lamination, and chaotic advection. The proper lamination could be achieved by a good combination of rotation and SAR. ISLM shows the best mixing performance, particularly at low *Re* for channels with low aspect ratio.
- Particularly, the twisting and lamination performances of STL and ISLM, respectively, depend on the channel aspect ratio as a result of rotations.

The present results provide fundamental characteristics of TSM which can be further utilized not only for the mixing but also for other microfluidic applications such as particle transport and sorting, flow manipulations, and so forth.

Acknowledgments

The authors thank the Korean Ministry of Commerce, Industry, and Energy for financial support via the Development of Next-Generation New Technology Program.

Literature Cited

1. Stroock AD, Dertinger SKW, Ajdari A, Mezić I, Stone HA, Whitesides GM. Chaotic mixer for microchannels. *Science*. 2002;295:647–651.
2. Nguyen N-T, Wu Z. Micromixers—a review. *J Micromech Microeng*. 2005;15:R1–R16.
3. Hessel V, Löwe H, Schönfeld F. Micromixers—a review on passive and active mixing principles. *Chem Eng Sci*. 2005;60:2479–2501.
4. Liu RH, Stremler MA, Sharp KV, Olsen MG, Santiago JG, Adrian RJ, Aref H, Beebe DJ. Passive mixing in a three-dimensional serpentine microchannel. *J Microelectromech Syst*. 2000;9:190–197.
5. Kim DS, Lee SH, Ahn CH, Lee JY, Kwon TH. Disposable integrated microfluidic biochip for blood typing by plastic microinjection mouldin. *Lab Chip*. 2006;6:794–802.
6. Aubin J, Fletcher DF, Bertrand J, Xuereb C. Characterization of the mixing quality in micromixers. *Chem Eng Technol*. 2003;26:1262–1270.
7. Kang TG, Kwon TH. Colored particle tracking method for mixing analysis of chaotic micromixers. *J Micromech Microeng*. 2004;14:891–899.

8. Ansari MA, Kim K-Y. Shape optimization of a micromixer with staggered herringbone groove. *Chem Eng Sci*. In press.
9. Schönfeld F, Hessel V, Hofmann C. An optimized split-and-recombine micro-mixer with uniform 'chaotic' mixing. *Lab Chip*. 2004;4: 65–69.
10. Schönfeld F, Hardt S. Simulation of helical flows in microchannels. *AIChe J*. 2004;50:771–778.
11. Jiang F, Drese KS, Hardt S, Küpper M, Schönfeld F. Helical flows and chaotic mixing in curved micro channels. *AIChe J*. 2004;50:2297–2305.
12. Mengeaud V, Josserand J, Girault HH. Mixing processes in a zigzag microchannel: finite element simulations and optical study. *Anal Chem*. 2002;74:4279–4286.
13. Vijayendran RA, Motsegood KM, Beebe DJ, Leckband DE. Evaluation of a three-dimensional micromixer in a surface-based biosensor. *Langmuir*. 2003;19:1824–1828.
14. Kim DS, Lee SH, Kwon TH, Ahn CH. A serpentine laminating micromixer combining splitting/recombination and advection. *Lab Chip*. 2005;5:739–747.
15. Park JM, Kim DS, Kang TG, Kwon TH. Improved serpentine laminating micromixer with enhanced local advection. *Microfluid Nanofluid*. In press.
16. Xia HM, Wan SYM, Shu C, Chwe YT. Chaotic micromixers using two-layer crossing channels to exhibit fast mixing at low Reynolds numbers. *Lab Chip*. 2005;5:748–755.
17. Xia HM, Shu C, Wan SYM, Chew YT. Influence of the Reynolds number on chaotic mixing in a spatially periodic micromixer and its characterization using dynamical system techniques. *J Micromech Microeng*. 2006;16:53–61.
18. Chen H, Meiners J-C. Topologic mixing on a microfluidic chip. *Appl Phys Lett*. 2004;84:2193–2195.
19. Hwang WR, Kang KW, Kwon TH. Dynamical systems in pin mixers of single-screw extruders. *AIChE J*. 2004;50:1372–1385.
20. Hughes TJR, Franca LP, Hulbert GH. A new finite element formulation for computational fluid dynamics. VIII. The Galerkin/least-squares method for advection–diffusion equations. *Comput Methods Appl Mech Eng*. 1989;73:235–255.
21. Franca LP, Frey SL. Stabilized finite element methods. II. The incompressible Navier-Stokes equations. *Comput Methods Appl Mech Eng*. 1992;99:209–233.
22. Ottino JM. *The Kinematics of Mixing: Stretching, Chaos and Transport*. New York: Cambridge University Press, 1989.
23. Hobbs DM, Muzzio FJ. The Kenics static mixer: a three-dimensional chaotic flow. *Chem Eng J*. 1997;67:153–166.
24. Hobbs DM, Muzzio FJ. Reynolds number effects on laminar mixing in the Kenics static mixer. *Chem Eng J*. 1998;70:93–104.

Manuscript received Jan. 4, 2008, and revision received Apr. 23, 2008.